SAURON

Using Saturn's Rings as a Cosmic Laboratory

Audrey Aebi, Camille Chatenet, Alexia Duchene, Fernando Gámez Losada, Jaroslaw Gierulski, William Hickmott, Hedvig Ihrlund, Dabrowka Knach, Luis Langermann, Dominic Locks, Aristeidis Polychronakis, Lidia Ramírez Arroyo, Leonard Schirner, Sabrina Sughi, Hugo Testa

Tutors: Riccardo Lasagni Manghi and Elise Wright Knutsen

16th of July 2025

Abstract

SAURON is a mission proposal that aims to unravel key processes that govern the early stages of planet formation. SAURON will investigate the complex physical environment of Saturn's rings as a natural laboratory for investigating mechanisms analogous to those in the protoplanetary disks. This mission will examine the frequency and outcomes of collisions, aggregation, and fragmentation of small bodies within the dense ring system. These processes are thought to play an important role in the early stages of disk evolution during planet formation. The proposed mission is a Radioisotope Thermoelectric Generator powered spacecraft equipped with two systems of stereo cameras (Wide Angle Camera and Narrow Angle Camera), a spectro-polarimeter, radio occultation and Dust Analyser to observe the processes of growth and fragmentation of particles and boulders within the rings. Observing these processes within the uniquely accessible environment of Saturn's rings offers an opportunity to improve our understanding of the processes that form planets in debris disks.

1 Science background

Protoplanetary disks (PPDs) are rotating, flattened structures of gas and dust that surround newly formed stars. These disks are the natural by-product of angular momentum conservation during the gravitational collapse of molecular clouds and they serve as the birthplace of planetary systems. Typically extending up to hundreds of astronomical units (AU) in size, PPDs are composed primarily of molecular hydrogen, along with trace amounts of heavier elements and dust grains. Over time, these dust grains collide and coalesce, eventually forming planetesimals and, under the right conditions, full developed planets.

Several critical physical processes govern the evolution of PPDs; viscous accretion transports angular momentum outward, allowing gas to spiral inward toward the central star. Simultaneously, magnetohydrodynamic (MHD) effects—including magnetic braking, the magneto-rotational instability (MRI), and magnetically driven winds—play a major role in regulating disk turbulence and angular momentum transport. Radiative heating and cooling, along with chemical reactions and dust grain evolution (e.g., coagulation, fragmentation, and migration), also shape the thermal and compositional structure of the disk Morbidelli et al. 2024. Together, these mechanisms set the stage for planet formation and strongly influence the architecture of emerging planetary systems.

Saturn's rings, despite being largely devoid of gas, offer a unique analogue to mechanisms in certain stages in the evolution of PPDs, especially in their transition to debris disks. While traditional PPDs are rich in gas and dust and actively forming planets, Saturn's rings more closely resemble protoplanetary debris—structures that may result after the dissipation of gas, where solid-body dynamics become dominant. The exact origin of Saturn's rings remains a topic of active research. Some studies (e.g. (Tchernyi, 2010)) propose the rings may have originated from remnants of the protoplanetary cloud itself, reinforcing the relevance of using the rings as a comparative system. Furthermore, Wyatt (2014) outlines the distinctions between gas-rich PPDs and debris disks, situating Saturn's rings within the latter category.

The dense and highly collisional environment of Sat-

urn's rings makes them an exceptional natural laboratory for studying disk dynamics in situ, surpassing what is possible in other small-body populations like the asteroid belt. As highlighted by Rein (2010); Burns and Cuzzi (2006), these rings serve as a valuable proxy for processes such as collisional damping, self-gravity wakes, and angular momentum transport that are otherwise currently impossible to observe directly in distant PPDs.

Planetary rings are more than visually striking structures—they are dynamic systems governed by physical processes that seem to be relevant to planetary formation. When studied up close, rings reveal a complex environment shaped by collisions, aggregation, and fragmentation, making them valuable analogues for other flattened cosmic structures such as protoplanetary and debris disks. Their unique combination of high particle density, continuous evolution, and observational accessibility makes them ideal for investigating the building blocks of planet formation.

Cassini-Huygens mission (2004–2017) offered the most detailed and transformative view to scientists (Dougherty et al. 2009). It was able to study the rings from multiple angles, wavelengths, and distances. These observations revealed that the rings are not solid structures but rather composed of countless icy particles ranging in size from micrometres to kilometres (Cuzzi et al. 2009). One of Cassini's major scientific contributions was demonstrating that Saturn's rings are active and evolving. Through observations like stellar occultations, radio and optical scattering, and infrared spectroscopy, it was possible to estimate particle sizes, compositions, and the vertical thickness of the rings. During Cassini's last orbits larger structures; so called *propeller moonlets* due to their perturbation within the ring migration; in the rings were observed (Spahn and Sremcevic (2000); Edgington and Spilker (2016)). More than 150 objects with this shape were identified and are mainly concentrated in the mid-A-ring (Tiscareno et al. (2008)), as they exist only in rings with width greater than 50 kilometres (Tiscareno et al., 2010). Spiral density waves of moderate strength can locally disturb the propeller population by raising collision speeds and may interfere with the formation of self-gravity wakes. Interactions generate strong brightness fluctuations at visible wavelengths due to macroscopic particles Tiscareno et al. (2010) around proto-moonlets that range in size between a hundred metres and a kilometre. Material increases the optical depth through interactions with light and this phenomenon and the same shape are modelled in N-body simulations Tiscareno et al. (2010) and protoplanetary simulations Latter et al. (2018), but for fewer particles as simulations become too computationally expensive for us to be able to understand all complex interactions of this formation highlighting the necessity for observational efforts.

2 Science case

Experiments conducted on Earth and aboard the Internation Space Station have provided valuable insights into the behaviour of particles ranging from μm to cm—particularly how they collide, stick together, or fragment (dust coagulation). At the other end of the scale, previous missions such as Cassini, along with ground-based and space telescopes (e.g., ALMA Wilson et al. 2019), have helped us understand large-scale processes like gravitational clumping and the formation of larger structures. However, the intermediate size range, from 10 cm to 10 m, remains poorly understood and largely unobserved. This is the fundamental knowledge gap that the SAURON mission aims to address by focussing on direct observations where laboratory study alone cannot provide the answers readily.

2.1 Mission goal

The SAURON mission shall investigate the physical mechanisms operating within Saturn's rings that can be considered analogous to those in protoplanetary debris disks. By gaining insights into these processes, this study will significantly advance our understanding of planetary formation within the Solar System utilising the interactions of pebbles and small bodies.

2.2 Science objectives

In order to achieve the mission goal (**SO**), the following objectives were developed.

SO-1: Investigate the physical and chemical properties of objects in Saturn's rings.

- Characterise the size distribution of agglomerates.
- Study physical and chemical properties of particles in the outer rings.
- Investigate the location, abundance, lifespan, and formation/destruction processes of moonlets.

SO-2: Study mechanisms leading to planetesimal formation in the wake regions of propeller moonlets.

- Examine different types (coagulation, bouncing, abrasion, fragmentation) of agglomerate collisions and their frequency.
- Investigate agglomerate growth barriers and the influence of volatile content.

Additionally, opportunistic science (OS) may be conducted using the instruments outlined in Section 3 and the orbital configuration described in Section 4. Such investigations are considered secondary and will in no way influence or drive the primary mission design. All OS activities will be limited strictly to the capabilities of the payload already selected to fulfil the core scientific objectives, ensuring that the mission remains fully optimised for its principal goals.

OS: Study density variations in Saturn's uppermost atmosphere.

- Study Saturn's atmosphere using remote radio occultation
- Examine variations in the local density of the uppermost atmosphere by measuring in-situ drag force during aerobraking manoeuvrers with accelerometers (described in detail in section 4.2).

2.3 Key requirements

To link the scientific objectives to the mission payload, the key measurement requirements for each instrument are briefly outlined. The particle size distribution within the rings is to be characterised using multiple instruments. At the microscopic scale, measurements will be carried out by the spectropolarimeter and the dust analyser, while the mm to m range will be covered through radio occultation and stereo imaging from the Narrow-Angle Camera (NAC) and Wide-Angle Camera (WAC) systems. Chemical and physical properties of the ring particles will be derived using data from the spectropolarimeter and dust analyser. Finally, the study of collisional processes—including collision types, growth barriers, and interactions involving moonlets—will be enabled by high-resolution imaging through the NAC and WAC systems.

Table 1: *Science Objectives and their instruments*

SO.1.1:	**Size Distribution of particles**
0.01–10 μm	Dust Analyser
0.1–10 μm	Spectro-polarimeter
1–50 mm	Radio Occultation
0.4–10 m	NACs
1–100 m	WACs
SO.1.2:	**Chemical and Physical Particle Properties**
Velocity	Dust Analyser
Charge	Dust Analyser
Isotopic Ratios	Dust Analyser
Composition	Dust Analyser & Spectro-polarimeter
SO2.1:	**Collision types**
Velocity	NACs
Radius 0.15 - 250 m	NACs
Radius 0.4 - 1400 m	WACs
SO2.2:	**Growth Barriers**
Velocity	NACs
Radius 0.15 - 250 m	NACs
Radius 0.4 - 1400 m	WACs

3 Instrumentation

3.1 Stereo Camera Systems Unit

The camera subsystem consists of two WACs and two high-resolution NACs, which can operate independently to capture images. When used in conjunction, they form a stereo system capable of reconstructing the distance to the object, allowing the scaling of 2D acquisitions into 3D measurements. Both the WAC and NAC are based on the SamCam and PolyCam instruments from the OSIRIS-REx mission (Rizk et al., 2017), but the optics and focal lengths have been adapted to meet the specific scientific requirements.

The WAC is a 20 mm F/3.5 telescope, with a pixel resolution of 200 µrad and a field of view (FoV) of 11.7°. It is equipped with a 1024^2 CCD detector covering the 200 - 900 nm spectral band, and has a mass of 2.58 kg.

The NAC is a 203 mm F/3 telescope with a mass of 9 kg. It provides a pixel resolution of 13.5 mrad and a FOV of 13°. It mounts a 4096^2 CMOS detector operating in the 200–900 nm range, allowing for high-resolution imaging across a wide field.

Two different modes are planned with the Stereo Camera System Unit during the science operations. The first is the scanning mode which uses the two WACs and NACs camera at over 8 frame per second (fps) to cover a large section of the rings and measure the size distribution of objects. The scanning with the WACs enable to detect and identify large key features, as Propeller moons. The second mode is the tracking mode which make use of one WAC and one NAC to track objects previously detected as key features. The camera can track objects during 5 to 8 seconds, and will enable to observe collisions over 2.5 cm/s.

Table 2: *Instruments and their functions*

Instrument	Principle	Particle Size	Wavelengths	Heritage
WACs	remote	m-km	0.28 - 0.9 μm	Cassini
NACs	remote	cm-m	0.28 - 0.9 μm	OSIRIS-REx
Spectro-polarimeter	remote	μm	0.35 - 5.1 μm	PACE SPEXone
Radio Occultation	remote	mm - cm	$\sim$1 cm & $\sim$4 cm	JUICE
Dust Analyser	in situ	μm	-	Europa-Clipper

3.2 Spectro-polarimeter

The spectro-polarimeter proposed for this mission is based on the SPEXone (PACE) instrument (Campo et al. 2018; van der Schaaf et al. 2024) and is designed to perform multi-angle, multi-spectral measurements of both radiance and degree of linear polarisation of sunlight scattered by Saturn's rings. Operating over a spectral range of 0.35μm to 5.1μm, the instrument features a pushbroom configuration with five viewing angles and a spectral sampling step of approximately 4 nm. The relative velocity between the spacecraft and the rings ($\sim$ 6 km/s) combined with a sampling rate of 2 Hz. The primary objective is to retrieve the size distribution and the composition of ring particles in the micrometer scale, see Muñoz et al. 2021.

3.3 Radio Occultation

The Radio Science Experiment will measure the density of mm to cm-sized particles in the rings by transmitting a sinusoidal signal through the Ka-band and X-band telecommunication channels. As the signal passes through the rings, its scattering and attenuation, observed in the frequency content of the signal received at the ground station Asmar (n.d.), reveal the size distribution of these particles. This technique, also used in missions such as Cassini, Voyager, and JUICE, enables analysis of particle density as a function of radius.

3.4 Dust Analyser

The dust analyser operates as a time-of-flight mass spectrometer, much like the EUROPA Clipper SUDA instrument described by Kempf and al (2025), but optimised for isotropic particle detection. Incoming dust grains from any direction are first accelerated through a uniform electric field, then their time-of-flight to a detector array yields both mass and velocity information. Compared to Cassini's CDA, our design features a wider acceptance angle for truly all-sky sampling, enhanced mass resolution through improved ion optics, and on-board event clustering to filter out background noise.

4 Trajectory design

To reach our target science orbit a series of phases, each comprising different orbital manoeuvrers, has to be executed. The following subsections elaborate on each phase.

4.1 Transfer to Saturn

Our low-thrust transfer trajectory to Saturn is based on the work presented by Fantino et al. (2023). The authors manage to deliver 1014 kg to Saturn's sphere of influence with an hyperbolic excess velocity of just $V_\infty = 1\,\mathrm{km\,s^{-1}}$ in 12.34 years. They use a low-thrust Earth-Venus-Venus-Earth-Saturn multi-gravity assist trajectory using an ion engine with a thrust level of 36 mN at 640 W. The launch mass is 1500 kg with a V_∞ from Earth of 5.2 $\mathrm{km\,s^{-1}}$, achievable with the Ariane 64 rocket.

4.2 Insertion Manoeuvrer

After arrival at Saturn, an insertion manoeuvrer, whose constituting steps can be seen in Fig. 1, has to be performed. Note that the figure is a schematic of the whole insertion process (not to scale). The following list links the colour code in the figure with the various steps:

- Saturn injection manoeuvrer (dark red)
- Start aerobraking (light blue)
- Crank manoeuvrer with Titan flyby (dark blue)
- Continue aerobraking (orange)
- Injection into science orbit (green)

First, the **Saturn injection manoeuvrer** (dark red) (i.e., $\Delta V = 186\,\mathrm{m\,s^{-1}}$ at the hyperbola's perikrone $r_p = 65\,000$ km) places the spacecraft into a highly elliptical orbit ($e = 0.98$). The feasible arrival dates match Saturn's solstices (earliest feasible arrival date March 5, 2075). The incoming hyperbola is contained in the ecliptic plane, meaning that in Saturn's equatorial reference frame, the resulting highly elliptical orbit has an inclination of 26.73° with the line of nodes parallel to the intersection between the ecliptic and Saturn's equatorial plane.

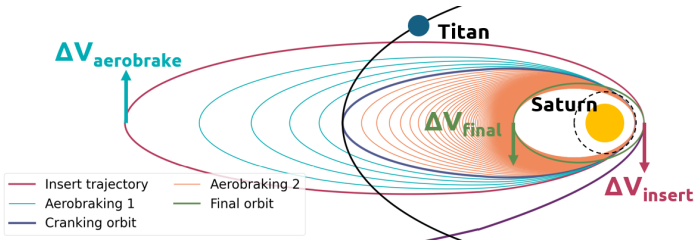

Figure 1: *Schematic depicting the various steps of the insertion manoeuvrer.*

After injection, the orbit's perikrone is lowered from 6500 to 61 168 km, into Saturn's atmosphere, via a $\Delta V = 10\,\mathrm{m\,s^{-1}}$ burn at the apokrone. This marks the **start of the aerobraking** manoeuvre (light blue), the objective of which is to lower the orbit's apoapsis to the target altitude by exploiting atmospheric drag. Given the high uncertainties of Saturn's atmosphere, the aerobraking manoeuvrer is done carefully, with the entire process taking roughly 400 days. The total ΔV gain is of the order of $5.5\,\mathrm{km\,s^{-1}}$, demonstrating the necessity of using aerobraking to reach the target science orbit. A preliminary analysis of the thermal conditions occurring during aerobraking, done using atmosphere model data derived by Yelle et al. (2018), indicate that the maximum heat fluxes do not exceed $54\,\mathrm{W/cm^2}$. For reference, this value is one fourth of the design heat flux for the Mars Science Laboratory lander Edquist et al. (2014). The value of $54\,\mathrm{W/cm^2}$ is the design load for the heat shield, which has been sized to be a 3 cm thick shield of PICA material.

During the aerobraking manoeuvrer, the apokrone slowly decreases until Titan's orbit is intersected. At that moment, Titan's gravity is exploited to perform a flyby, **cranking the orbit** close to the orbital plane (dark blue) (i.e., a gravity assist $\Delta V = 700\,\mathrm{m\,s^{-1}}$ cranks the orbit from 26.73° to 0.006°). The low but non-zero inclination ensures close proximity to Saturn's rings while avoiding collisions with the ring particles. The impact parameter for the flyby is 5600 km, which yields a periapsis from Titan of 5000 km, high enough to avoid collision with Titan (i.e., radius of 2574.7 km). The required turning angle of the relative velocity vector is 11.1°.

After the cranking, **aerobraking is resumed**, further lowering the apokrone up to the outer rim of ring F (orange). At the target apokrone of $r_a = 141\,750$ km the last impulsive manoeuvrer (i.e., $\Delta V = 200$ m s) is executed to **raise the perikrone** to 65 000 km out of the atmosphere, effectively ending the aerobraking manoeuvrer and inserting the spacecraft into the target science orbit (green).

4.3 Science Orbit

The science orbit is designed to ensure that the vertical distance from the plane of the rings when the spacecraft transits over the rings is lower than 10 km. Additionally, the orbit has to avoid colliding with the rings themselves. An inclination of 0.006°was selected to fulfil both criteria (i.e., minimum vertical distance of 3.8 km). The nodes of the orbit are placed in the gap between Saturn and the innermost ring and in the outer rim of ring F, respectively (i.e., $r_p = 65\,000$ km and $r_a = 141\,750$ km). Because the orbit is elliptical and the particles in the rings travel in circular orbits, the orbital velocities differ, yielding an average relative velocity of $6.5\,\mathrm{km\,s^{-1}}$. The orbital period is 9 h and 30 min, from which 6 h is spent over / below the rings.

4.4 Delta-V budget

Table 3 gathers all the required velocity changes and the associated propellant consumption for each manoeuvre. The remaining propellant is also included. With the current design, we have 170 m/s left for station keeping and desaturation of the reaction wheels.

Table 3: *Delta-V budget.*

Manoeuvre	ΔV ($\mathrm{m\,s^{-1}}$)	Used (kg)	Left (kg)
Pre-launch		N/A	664
Earth to Saturn	5372	470	194
Saturn injection	180	62	132
Start aerobraking	10	3	129
Aerobraking	5500	0	129
Cranking	700	0	129
Science injection	200	68	61
Station keeping	170	61	0

5 Spacecraft

The SAURON spacecraft dimensions are 1.5 x 1.5 x 2.5 m (w x h x l). It is composed of a satellite bus to host the scientific instruments and the components necessary to support the operations. The Stereo Camera System Unit and spectro-polarimeter are mounted on the same side of the spacecraft facing Saturn's rings. The dust analyser is placed in the direction of the spacecraft velocity in order to collect the dust particles.

The dry and wet mass of the SAURON spacecraft are 950 kg and 1108 kg, respectively. A margin of 5 % to 20 % has been added to each equipment according on their

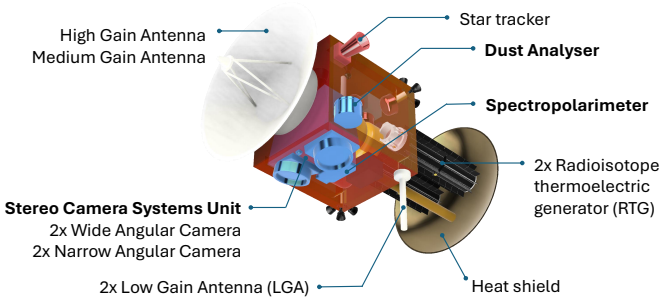

Figure 2: *SAURON spacecraft preliminary design*

maturity, and an additional 20 % margin to the subsystem. The propellant margin is calculated with 10% margin.

Table 4: *Spacecraft mass budget*

Subsystem	Mass (kg)	System margin
Payload	40.82	51.45
Power	176	232.32
Communications	65	85.5
Thermal	70	89.4
Propulsion	87.1	110.6
Structures	160	230.4
AOCS	38.2	48.9
C&DH & Harness	79.7	100.4
Total dry mass		949.1
Propellant		158.6
Total wet mass		1107.6

5.1 Structures and Mechanism

The SAURON spacecraft has been designed to have a stable aerodynamic shape to withstand high torques and stresses during the aerobraking manoeuvre. The spacecraft structure is made of a rigid aluminium frame. The frame supports the scientific payloads and the satellite subsystems and protects them during the launch and the space environment. The main frame is the shape of a rectangular box of 1 x 1 x 1.5 m. The structure hosts the propellant tanks and engine thrusters (propulsion subsystem), sensors and actuators for the attitude control, a battery, on-board computer, and the scientific instrumentations (dust analyser, spectro-polarimeter, and the Stereo Camera System Unit).
A side of the main bus is dedicated to the mounting of the two radioisotope thermoelectric generator (RTG), and the heat shield. On the opposite side, the high gain antenna (HGA) is mounted on a gimbal system to communicate with Earth during the science operations.

5.2 Propulsion

The main requirement of the propulsion system is to provide the spacecraft with sufficient capabilities for orbital manoeuvring and attitude control.

The system should also allow for completing the interplanetary MGA trajectory from Earth to Saturn. Currently, the most advanced method for reaching such distances is via the use of low thrust propulsion engines. In this case, as mentioned in section 4.1, a PPSX00 Hall-effect thruster providing an Isp of 1400 s and a thrust of 36 mN is used. The entire low-thrust phase uses 486 kg of Xenon propellant, for which a high pressure tank weighing 44 kg is used.

Once at Saturn however, the successful execution of fast, impulsive-like injection and orbit correction manoeuvrers, necessitates the use of higher thrust propulsion methods. SAURON uses chemical propulsion, namely a set of six 10 N, 300 s Isp bi-propellant thrusters, using MMH / N2O4 as fuel/oxidiser. This configuration allows for the performance of 17 minute injection manoeuvrer into Saturn's orbit (Cassini's manoeuvrer lasted over an hour), which is satisfactory for the mission's needs. The tank for the chemical propulsion was sized to be roughly 20 kg. These thrusters will also be used for tasks related to station keeping, such as reaction wheel desaturation and atmospheric / particle drag compensation.

Because of time constrains, the option to combine AOCS and chemical propulsion systems, similar to ESA's Rosetta mission, was not fully explored. This is suspected to be a potential avenue for mass reduction in later concept analysis.

5.3 Attitude and Orbit Control System (AOCS)

AOCS is a necessary subsystem to achieve the scientific requirements. Attitude control shall satisfy the pointing and stability requirements imposed by the scientific objectives and satisfy the functional needs of the platform subsystems: communication links, thermal control, and orbit control.

In the Saturn environment, the maximum external torque is due to the magnetic torque (10^{-4} N.m). The aerodynamic torque has been measured from the atmospheric density of Saturn. The aerodynamic torque becomes stronger than the magnetic torque for very low altitude of 2 km above the 1-bar atmospheric reference level. The spacecraft reaches this altitude at the periapsis

distance, but does not decrease below this altitude. The external torque due to solar radiation and the gravity gradient are of 1×10^{-5} N m and 1×10^{-8} N m, respectively.

The camera science operations require a pointing accuracy of 0.3° to achieve the stereo images. This accuracy represents an error of 10% of the footprint camera length. In addition, the satellite needs to be reoriented at an angular speed of $11.5°/s$ during 8 seconds to follow its target during the tracking mode. To fulfil these requirements, sensors and actuators are required in a closed loop system. A star tracker and three Inertial Reference Unit (IRU) (gyroscopes and accelerometers) are used to determine the position and orientation of the spacecraft. The attitude is controlled by 4 reactions wheels (1 for redundancy) in a pyramid configuration. The reaction wheel will need to provide enough torque to fulfil the slewing rate of the spacecraft and further iterated in Phase B. The reaction wheels are complemented by 6 cold gas thrusters for momentum offloading and manoeuvrers during the science operations.

5.4 Thermal control system

The principle challenges are the very cold environment of Saturn, while also being able to handle the warm environment of Venus on flybys. Because of the range of wavelengths used for the observations, no instrument needs to be actively cooled. Therefore, the aim is to keep the entire spacecraft and electrical components within an acceptable range of temperatures.

As a first approximation, the S/C was considered as an aluminium cube of 1 m long with 2 antennas. RTGs cooling is assumed to prevent the generated heat from spreading within the spacecraft. A single-node thermal equilibrium—involving the solar flux, planetary IR emission, albedo, and internal power dissipations—has been done for 3 different boundary cases:

1. Flyby close to Venus considering the maximum power consumption during orbit transfer,
2. Cold operation case in eclipse during the orbit around Saturn considering the minimum power consumption,
3. Hot operation case in sunlight during the orbit around Saturn considering the maximum consumption power.

Table 5 provides a summary of the computed S/C temperatures for each case considered. It appears that no radiator is needed to evacuate heat during Venus flyby, but local electrical heating and MLI will be required for the most critical component during the coldest operation phase.

Table 5: *Computed S/C temperature for 3 different boundary cases*

Venus flyby	Cold Operation	Hot Operation
−31.7 °C	−102.7 °C	−4.6 °C

5.5 Power

The spacecraft power budget has been analysed for four mission phases: LEOP, interplanetary transfer, measurement mode, and downlink mode. Of these, the most demanding by far is the interplanetary transfer phase, shown in Table 6. It is dominated by the requirements of the Ion engines, which require 660 W of power for the interplanetary transfer trajectory. Providing this amount of power at Saturn is not feasible using solar panels, as the required area would be on the order of multiple hundreds of square meters, which is unsustainable from a mass- and volume budget point of view, as well as from a risk analysis standpoint while operating so close to the rings. Thus, the only viable solution is to use radioisotope thermal generators (RTGs).

For this purpose, NASA's Next Generation RTGs, which are currently under development and expected to first launch 2030, are selected. They are assumed to be scalable proportionally to the required power draw, which is distributed over two separate units for to symmetrically distribute the weight and provide redundancy.

Due to the high reliability and constant uptime of this power source, very little gaps in supply are expected. Therefore, a small 200 W h Li-SO2 battery should be sufficient to handle small sudden peaks in power demand.

Table 6: *Power Budget in Watt*

Subsystem	Power Transfer (W)
Payload	0
Comms	2
Thermal	10
Propulsion	660
C&DH + harness	30
Structure	0
AOCS	26.52
Total	**728.52**

5.6 Command and Data Handling (C&DH)

The C&DH subsystem is configured to reconcile the substantial data volume generated by the payload suite with the limitations imposed by intermittent downlink opportunities. A radiation-hardened flight processor communicates over a redundantly routed SpaceFibre switch fabric

with an FPGA-based collision processing unit that incorporates a lightweight neural network. In real time, WAC and NAC frames are analysed: individual particles are identified, their principal attributes—position, velocity, size, and intensity—are extracted, and full-frame images are discarded immediately unless explicit ground-segment approval for retention has been granted. Extracted metadata are packeted and subjected to CCSDS-style lossless compression before being committed to a three-tier storage architecture.

Tier one comprises a high-throughput burst buffer (2×16 GB RAID-1), optimised for rapid ingress and egress of compressed camera outputs. Tier two is constituted by a 64 GB temporary buffer, which retains processed metadata and, upon receipt of ground commands, selected full-frame data pending authorisation. Tier three consists of a long-term archive (2×1 TB RAID-1) that preserves all processed metadata indefinitely, along with any raw imagery explicitly designated for later retrieval.

During science-mode operations, approximately one third of each orbit is allocated to communications. Within this interval, a downlink budget of 65.5 MB is enforced, of which 4 MB support housekeeping and standard telemetry and 2 MB underpin the ground-in-loop catalogue. The remaining 61.5 MB is dedicated to science products, with roughly 70% of that volume earmarked for ground-requested datasets and the balance reserved for burst-mode observations or unplanned retransmissions. Additional bandwidth for larger dataset transfers may be scheduled during non-science or reduced-science mode orbits. By integrating in situ neural-network processing, adaptive lossless compression and a tiered storage strategy, the OCDH subsystem ensures strict compliance with downlink constraints while maintaining the capability to recover full-resolution datasets on demand.

5.7 Telemetry, Tracking, and Command (TT&C)

The TT&C system is responsible for maintaining the telemetry, telecommand, and data downlink capabilities of the spacecraft. Additionally, it provided ranging and Doppler-based velocity measurement, and is used in the Radio Science Experiment. It operates a total of four antennas, each required in a different phase of the mission.

First, two S-band low-gain antennas (LGA) are used during the LEOP phase to provide initial communication with the spacecraft after launch. Due to their omnidirectional pattern and low power requirement, they pose very little requirements on the other spacecraft subsystems and can be used to reliably power-on and test the other subsystems while in the vicinity of Earth. They may additionally be used in the inner solar system part of the interplanetary trajectory, as these mission phases have low data requirements and the close proximity to the sun has been shown in similar previous missions to pose some difficulties to the main antenna.

The main antenna is a high-gain antenna (HGA) operating in X- and Ka-Band. The RF system is composed of a 2m-diameter parabolic reflector, a 100 W travelling wave tube amplifier, and RF transponder. While the Ka-band channel is used for high-throughput bulk data transfer, the X-band is transmitted simultaneously to provide a redundant channel with much lower pointing requirements, supply calibration information for the Doppler, and can be used for the Radio Science Experiment. For this purpose, it is fed by an ultra-stable oscillator.

Finally, a medium gain antenna (MGA) is used to provide a highly reliably but extremely slow communications channel in the case of being Sun-pointing during safe-mode. Following Cassini's example, it is mounted coaxially inside the reflector of the HGA dish.

The main design driver for this system is the bulk download of science. In this mode, the Ka-band antenna has the full availability of the pointing capabilities of the spacecraft, and transmits at maximum power down to one of the ESA ESTRACK 35 m antennas. The link budget for this scenario is shown in Table 7. It assumes a communication phase of 33 % of the total orbit, and a 50 % rate of availability of the ground station, due to time-sharing agreements, weather problems and similar.

Following the example of the BepiColombo mission, Turbo-code with code rate 1/2 and 8920 bit block size is used, lowering the required Eb/N0 for a bit error rate of 1×10^{-6} to only 1 dB, at the cost of higher bandwidth. Adaptive coding can be used to vary the channel parameters in case of interferences with the signal quality.

The system also provides TT&C to the spacecraft. For this purpose, it is mounted on a gimbal. This won't be used for bulk downlink during science mode due to coarser pointing accuracy (only for telemetry).

Currently not considered in this analysis are topics such as planetary atmospheric effects (both on Earth and Saturn, with the latter being additional scientific results gained during operations), interference from solar plasma plumes, etc. Additionally, data download during the science phase (beyond TT&C) is not considered, as the link budget presented here is sufficient to satisfy data budget requirements.

Table 7: *Link Budget Calculation*

RF Transmit Power	100 W
Transmitter Losses	0.9
Diameter	2 m
Efficiency	0.55
Frequency	32 GHz
Range	10 AU
Transmission Path losses	0.65
Rx G/T	55.8 dB
Pointing Loss	0.03°
Required Eb/N0	1 dB
Maximum Data Rate	77.5 kbps
Bulk download availability	16.66%
Data per Science Orbit	54.2 MB

6 Operations & Ground Segment

The Concept of Operations (ConOps) will consist of five phases. The mission commences with the Launch and Early Operations (LEOP), including a check-out phase and platform commissioning. Once the interplanetary trajectory is initiated, the mission enters the Transfer Phase, which will last 12 years. During the two year long Orbit Insertion Phase, the spacecraft will enter its nominal orbit around Saturn, thus commencing the Science Phase. After three years of operations, the mission ends with a final phase, End-of-Life, where the spacecraft is decommissioned. Should the conditions of the spacecraft allow, an extension of the operations is possible. This could then be an opportunity for extended science operations and an occasion for opportunistic science.

During this mission, the ESA ESTRACK 35 m antennas will be used for communication with the spacecraft using parabolic antennas. ESA's control centre will plan the operations, manage anomalies, and coordinate scientific observations, as an L-class mission 50 % availability is considered.

7 Technology Readiness Level

The Technology Readiness Levels (TRL) of the scientific instruments are of level 6 or above. The payload on-board have a high maturity and benefit of the heritage of previous space missions (OSIRIS-REx, EUROPA CLIPPER...). Further testing will be performed in Phase B and C to qualify the instrumentation for the Saturn environment.

Table 8: *Technology Readiness Levels of payloads.*

Instrumentation	TRL	adapted from
WAC	7	OSIRIS-REx
NAC	7	OSIRIS-REx
Spectropolarimer	6	PACE project
Dust analyzer	6	EUROPA CLIPPER

8 Timeline

The SAURON mission should begin with Phase 0 in 2045, focused on mission identification and preliminary analysis. This initial step is essential to clarify the scientific objectives and outline the fundamental requirements.

Two years after in 2047, **Phase A** will define the mission concept, assess its feasibility, and establish the initial system requirements.

Phase B in 2049 will consist of developing the preliminary design, including a comprehensive risk assessment and a more detailed definition of system requirements. We want two years for this phase.

Phase C in 2053, scheduled for 4 years, will involve developing the detailed design, finalizing subsystem designs, systems integration planning, and completing the critical design review.

Phase D in 2057 will also begin over 4 years, also covering qualification, production, system validation, assembly and integration, extensive testing, infrastructure acceptance, and full launch preparation.

Finally, **Phase E** starts in 2061 and will cover launch execution, commissioning, initial operations, routine monitoring, and end-of-life planning. After launch, our spacecraft will be in Saturn orbit on March 5th, 2075. The end of this phase should be in 2078 with the end of our mission. The mission may also be extended depending on system performance and scientific return.

9 Risk management

This mission is exposed to a number of fundamental risks. First and foremost using RTGs as a power-source and launching them exposes earth to the risk of multiple kgs of Plutonium in the atmosphere. However this catastrophic risk has been successfully mitigated in the past through protective casing, safety modelling, safe trajectories and destructive and non-destructive testing. Other fundamental risks are posed by collision with larger particles and too much heat-flow during aerobraking, both of these topics will have to be extensively studied and modelled

Table 9: *Mission timeline and segments*

Time	Mission Segment	Description
2046–2048	LEOP	Single Ariane Launch Checkout Phase
+12 years	Transfer	Low-thrust electric transfer on the interplanetary trajectory
+2 years	Orbit Insertion	Insertion into nominal Saturn orbit
+3 years	Science Phase	Four operational modes
Earliest: 2061	End of Life	Spacecraft decommissioning

before and during the mission. These and other risks are compiled in figure 3.

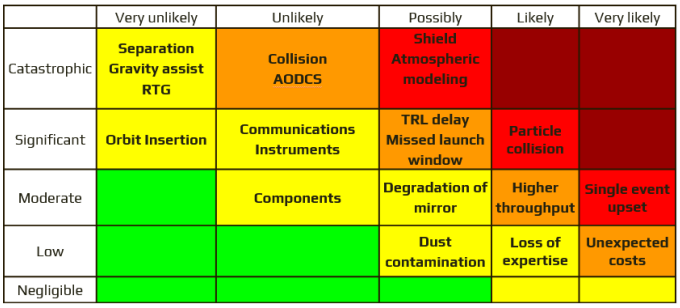

Figure 3: *The mission risks and their relative importance in terms of likeliness and impact.*

10 Cost

The SAURON mission is going to be an ESA L class mission. As shown in Table 10 the estimated cost at completion (CAC) is going to be around 1.1 billion euro. The launcher cost is estimated to be higher due to the RTGs as compared to other Ariane 64 launches.

11 Summary

SAURON is dedicated to in-depth exploration of Saturn's rings as a natural laboratory for studying key processes in planet formation. By observing how particles collide, grow, and break apart across a wide range of sizes, the mission will address one of the most critical gaps in our understanding: how small dust grains evolve into larger building blocks of planets. Saturn's rings offer a uniquely accessible environment to witness these processes in action, under conditions that closely resemble those in the early Solar System. SAURON is both challenging and ambitious, involving innovative approaches to observe fine-scale dynamics in a complex and fast-moving environment. Its discoveries will provide new insights into how planetary systems form, like our own and those around other stars.

Table 10: *SAURON Mission Budget*

Cost Category	**Cost (M€)**
ESA Mission Contribution	110
Spacecraft Development	300
RTGs (Power System)	250
Mission Operations	80
Science Operations	70
Subtotal	**810**
Contingency (15%)	121.5
Launcher (including RTG safety)	170
Total Cost at Completion	**1102**

References

Asmar, S. W. (n.d.), 'PDS3 Cassini Radio Science User's Guide', NASA Planetary Data System, urn:nasa:pds:misc:document_cassini:pds3_radioscience_ug_20180930::1.0.

Burns, J. A. and Cuzzi, J. N. (2006), 'Our local astrophysical laboratory', *Science* **312**(5781), 1753–1755.
URL: *http://dx.doi.org/10.1126/science.1114856*

Campo, J., van Amerongen, A., Rietjens, J., Dogan, E., Dingjan, J., Nalla, R., Caron, J. and Hasekamp, O. P. (2018), SPEXone: a Compact Multi-Angle Spectropolarimeter, *in* 'AGU Fall Meeting Abstracts', Vol. 2018, pp. A33H–3235.

Cuzzi, J., Clark, R. et al. (2009), Ring particle composition and size distribution, *in* 'Saturn from Cassini-Huygens', Springer Netherlands, Dordrecht, pp. 459–509.

Dougherty, M., Esposito, L. and Krimigis, S., eds (2009), *Saturn from Cassini-Huygens*, 2009 edn, Springer, New York, NY.

Edgington, S. G. and Spilker, L. J. (2016), 'Cassini's Grand Finale', *Nature Geoscience* **9**(7), 472–473.

Edquist, K. T., Hollis, B. R., Johnston, C. O., Bose, D., White, T. R. and Mahzari, M. (2014), 'Mars science laboratory heat shield aerothermodynamics: Design and reconstruction', *Journal of Spacecraft and Rockets* **51**(4), 1106–1124.

Fantino, E., Burhani, B. M., Flores, R., Alessi, E. M., Solano, F. and Sanjurjo-Rivo, M. (2023), 'End-to-end trajectory concept for close exploration of saturn's inner large moons', *Communications in Nonlinear Science and Numerical Simulation* **126**, 107458.

Kempf, S. and al, e. (2025), 'Suda: A surface dust analyser for compositional mapping of the galilean moon europa', *Space Science Reviews* **221**(1).

Latter, H. N., Ogilvie, G. I. and Rein, H. (2018), Planetary rings and other astrophysical disks, *in* 'Planetary Ring Systems', Cambridge University Press, pp. 549–576.

Morbidelli, A., Marrocchi et al. (2024), 'Formation and evolution of a protoplanetary disk: Combining observations, simulations, and cosmochemical constraints', *Astron. Astrophys.* **691**, A147.

Muñoz, O., Frattin, E., Jardiel, T., Gómez-Martín, J. C., Moreno, F., Ramos, J. L., Guirado, D., Peiteado, M., Caballero, A. C., Milli, J. and Ménard, F. (2021), 'Retrieving dust grain sizes from photopolarimetry: An experimental approach', *Astrophysical Journal Supplement Series* **256**(1), 17.

Rein, H. (2010), The effects of stochastic forces on the evolution of planetary systems and Saturn's rings, PhD thesis, University of Cambridge.

Rizk, B., d'Aubigny, C. D., Golish, D. et al. (2017), 'OCAMS: The OSIRIS-REx camera suite', *arXiv [astro-ph.IM]* .

Spahn, F. and Sremcevic, M. (2000), 'Density patterns induced by small moonlets in saturn's rings?', *Astronomy and Astrophysics, v. 358, p. 368-372 (2000)* **358**, 368–372.

Tchernyi, V. (2010), About separation and collision of Saturn rings particles, *in* '38th COSPAR Scientific Assembly', Vol. 38, p. 2.

Tiscareno, M. S., Burns, J. A., Sremčević, M., Beurle, K., Hedman, M. M., Cooper, N. J., Milano, A. J., Evans, M. W., Porco, C. C., Spitale, J. N. and Weiss, J. W. (2010), 'Physical characteristics and non-keplerian orbital motion of "propeller" moons embedded in saturn's rings', *The Astrophysical Journal Letters* **718**(2), L92.
URL: *https://dx.doi.org/10.1088/2041-8205/718/2/L92*

Tiscareno, M. S. et al. (2008), 'The population of propellers in saturn's a ring', *The Astronomical Journal* **135**(3), 1083.

van der Schaaf, L., Jonker, M., Laasner, R., Rietjens, J. H. H., Hasekamp, O. P., Vretenar, M., Tol, P. and Smit, M. (2024), Georegistration and viewport coregistration for spexone, the multi-angle spectropolarimeter on-board the nasa pace satellite, *in* T. Kimura, S. R. Babu and A. Hélière, eds, 'Sensors, Systems, and Next-Generation Satellites XXVIII', SPIE, p. 12.
URL: *http://dx.doi.org/10.1117/12.3031741*

Wilson, C., Dong, R., di Francesco, J., Fissel, L., Johnstone, D., Kirk, H., Matthews, B., McNamara, B., Rosolowsky, E., Rupen, M., Sadavoy, S., Scott, D. and van der Marel, N. (2019), Development Plans for the Atacama Large Millimeter/submillimeter Array (ALMA), *in* 'Canadian Long Range Plan for Astronomy and Astrophysics White Papers', Vol. 2020, p. 19.

Wyatt, M. (2014), Insights into planetary systems through JWST imaging of debris disks, *in* 'American Astronomical Society Meeting Abstracts #223', Vol. 223 of *American Astronomical Society Meeting Abstracts*, p. 314.04.

Yelle, R. V., Serigano, J., Koskinen, T. T., Hörst, S. M., Perry, M. E., Perryman, R. S. and Waite Jr., J. H. (2018), 'Thermal structure and composition of saturn's upper atmosphere from cassini/ion neutral mass spectrometer measurements', *Geophysical Research Letters* **45**(20), 10,951–10,958.